

Preparing undoped and Mn-doped ZnO nanoparticles: a comparison between sol–gel and gel-combustion methods

M. Ebrahimizeh Abrishami · A. Kompany ·
S. M. Hosseini · N. Ghajari Bardar

Received: 31 March 2011 / Accepted: 27 January 2012 / Published online: 11 February 2012
© Springer Science+Business Media, LLC 2012

Abstract Undoped and Mn doped ZnO nanoparticles were synthesized by two wet chemical techniques: sol–gel and gel-combustion. We were able to prepare Mn-doped ZnO nanoparticles free from the second phases at calcining temperatures 400 and 500 °C using sol–gel and gel combustion, respectively. Complete crystallization occurs in both methods, but it is found that the crystallization is better performed in the ZnO based solid solution prepared by the sol–gel method. TEM images show that the average size of the nanoparticles synthesized by gel-combustion is smaller than that of prepared by sol–gel method. Optical characterizations such as vibrational properties, lattice dynamical parameters, absorption edges and optical band gap energies were also carried out by FTIR and UV–Vis spectroscopies. The quantitative estimations led to the conclusion that the effects of the method on the particle size and the optical band gap energy of the prepared samples are very significant.

Keywords ZnO · Mn doping · Gel-combustion · Sol–gel · Optical properties

1 Introduction

ZnO based compositions have been used extensively in fabricating electronic and optoelectronic devices, due to

their applicable electrical and optical properties. It is obvious that the operation of ZnO based optoelectronic devices such as UV photo detectors and photodiodes depends on the optical properties of the samples in UV region. The effect of some dopant agents such as transition metals (Mn, Co, Ni, Fe, V) on the optical properties of ZnO has been studied by many researchers who found different or even antithetical results.

In preparing ZnO:Mn particles, it is very important to increase the solubility of Mn atoms in ZnO structure. Also, the synthesis method strongly affects the particle size, homogeneity of the particle size distribution and the shape of particles which results in distinguished changes in the properties. Brus [1] suggested a relation between particle size and optical band gap energy and Nepijko et al. [2] implied that the particle size might affect the lattice constants. Recently, several routes have been suggested for the synthesis of undoped and Mn-doped ZnO nanostructures, such as gel-combustion [3], sol–gel [4] and co-precipitation [5]. In the sol–gel method, the starting materials are dissolved and the obtained solution is then heated to evaporate the solvents and convert the sol into a viscous gel. Then, the gel is dried by increasing the temperature and the resulting product is calcined to obtain the desired nanostructure. In gel combustion method, the gel drying process is completed by using a fuel such as glycine or urea. In the case of preparing the ZnO:Mn nanostructures, changing the starting materials, thermal regime and the method used lead to different structural and morphological properties (Table 1).

In the present work, two simple techniques have been carefully studied for preparing ZnO:Mn nanoparticles. Also, studies on the changes of nanostructures properties due to the method of synthesis are put forward. Emphasis is put on the optical properties of Mn doped ZnO in UV and

M. Ebrahimizeh Abrishami (✉)
Department of Physics, University of Neyshabur,
Neyshabur, Iran
e-mail: ebrahimizeh@ymail.com

A. Kompany · S. M. Hosseini · N. Ghajari Bardar
Department of Physics (Materials and Electroceramics
Laboratory), Ferdowsi University of Mashhad, Mashhad, Iran

Table 1 The methods and starting materials which were used to prepare ZnO:Mn nanoparticles and their morphology

References	Method	Precursor materials	Morphology
[5]	Co-precipitation	Zinc chloride, distilled water, NaOH	Nanoparticle
[6]	Hydrothermal	Zinc foil	Nanorod
[7]	Hydrothermal	Zinc acetate, Monoethanolamine	Nanohollow
[8]	Sol-Gel	Zinc acetate, citric acid, ethanol	Nanobundle

mid-IR region. Overall, the changes in the structural and optical properties due to the synthesis technique and Mn doping levels are investigated. FTIR spectroscopy was applied to perform a subtle analysis on structure formation.

2 Experimental procedures

The precursors used for the synthesis of $Zn_{1-x}Mn_xO$ ($x = 0.00, 0.06, 0.10$) nanoparticles were zinc acetate dihydrate, $Zn(CH_3COO)_2 \cdot 2H_2O$ (Merck, 99.5%), manganese acetate tetrahydrate, $Mn(CH_3COO)_2 \cdot 4H_2O$ (Merck, 99%), acetic acid (Merck, 99.8%) and diethanolamine (DEA) (Merck, 98%). Appropriate amounts of zinc and manganese acetates were dissolved in a mixture of isopropanol and distilled water, stirring and heating at 40 °C for 30 min. Then, a mixture of acetic acid and DEA was added to the cations solution and the whole solution was continually stirred until it became clear with no precipitates and particulates. The molar ratio of acetic acid and DEA to cations was kept at two and unity, respectively. In order to obtain a clear sol, the obtained solution with $pH \approx 7$ was refluxed for 4 h at 110 °C. Then, a heat bath at 80 °C was used to evaporate the solvents until the desired gel was obtained. In this stage, two different routes were performed to dry the gel as follows:

1. In sol-gel method, the gel was dried by direct heating at 140–150 °C for 12 h.
2. In gel-combustion method, nitric acid was added as the fuel to the gel in order to complete the drying process. The molar ratio of the fuel to cations was chosen 2.5.

In the first procedure, performing the gel drying process took a long time, while the gel could be dried in few minutes by adding the suitable fuel. Finally, to determine the minimum calcining temperature needed in which the mono-phase nanopowders were obtained, the calcining process was performed for 2 h at different temperatures.

In this work, the crystal structure of the synthesized powders was characterized using X-ray diffraction (XRD) technique and the average particle size was obtained by

transmission electron microscopy (TEM). Fourier transmission infrared (FT-IR) spectra of the powders (as pellets in KBr) were recorded in the range of 400–2,000 cm^{-1} . The variation of the absorption edge and the band gap energy with changes in Mn content were investigated by UV-Vis absorption spectra recorded from nanopowder which has been ultrasonically dispersed in distilled water.

3 Results and discussions

3.1 Structural investigation

Figure 1 shows the XRD pattern of $Zn_{0.94}Mn_{0.06}O$ nanopowder obtained by sol-gel method after calcining the powders at 300 °C. This figure reveals that the sample is mostly crystallized in the wurtzite structure, but extra peaks related to tetragonal structure, are also observed [9]. In order to eliminate the secondary phase, the calcining temperature was increased to 400 °C. As shown in Fig. 2, the XRD patterns of $Zn_{1-x}Mn_xO$ ($x = 0.00, 0.06, 0.10$) nanopowders calcined at 400 °C show that the secondary phase is eliminated at this temperature. The wurtzite diffraction peaks are indexed in Fig. 2a. The characteristic peaks with the high intensity denote the complete crystallization process. These results show that the solubility of manganese in ZnO has been increased. Jayakumar et al. [10] reported the presence of the secondary phase in $Zn_{0.95}Mn_{0.05}O$ nanopowder, synthesized by co-precipitation method. According to Straumal et al. [5] studies, Mn solubility in ZnO structure depends on the particle size. Because of the tendency of Mn atoms to be collected at grain boundaries, the increase of Mn solubility with decreasing particle size is expected [5, 11]. As shown in Fig. 2, the increasing of Mn content in ZnO has two significant effects namely: broadening the peaks and shifting the peaks to lower angles which is shown by a guideline.

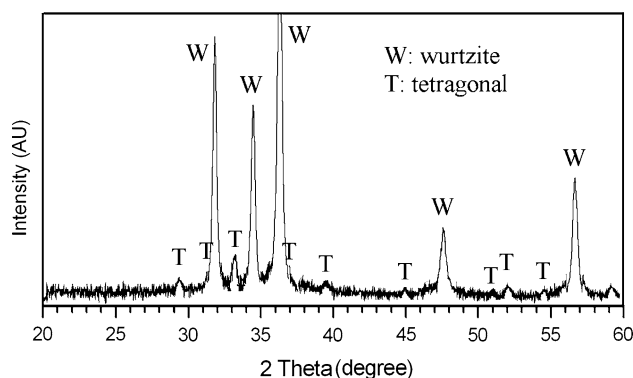


Fig. 1 XRD pattern of the $Zn_{0.94}Mn_{0.06}O$ nanopowder prepared by sol-gel technique. The calcining temperature was 300 °C

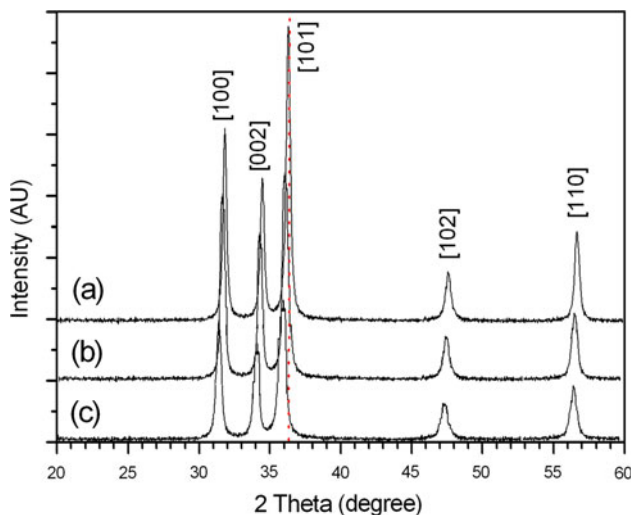


Fig. 2 XRD patterns of the $Zn_{1-x}Mn_xO$ nanopowders prepared by sol-gel technique: (a) $x = 0.00$, (b) $x = 0.06$ and (c) $x = 0.10$, calcined at $400\text{ }^\circ\text{C}$

The XRD patterns of $Zn_{0.94}Mn_{0.06}O$ nanopowder obtained by gel-combustion method calcined at 300 and $400\text{ }^\circ\text{C}$ are the same as Fig. 1 in which the reflectance peaks corresponding to the second phase exist. Consequently, the calcining temperature was increased up to $500\text{ }^\circ\text{C}$. The rate of heating and cooling of the calcining process was chosen exactly the same as the first method. Figure 3 displays the XRD patterns of $Zn_{1-x}Mn_xO$ ($x = 0.00, 0.06, 0.10$) nanopowders obtained at calcining temperature $500\text{ }^\circ\text{C}$. Obviously, this figure shows that the second phase is eliminated. In this case, the presence of the second phase in the $x = 0.06$ doped sample calcined at $400\text{ }^\circ\text{C}$ signifies that the sol-gel method is more reasonable for preparing mono-phase nanopowders at lower temperatures in comparison with the gel-combustion.

Figure 3 reveals that the broadening of the XRD peaks due to the increase of the amount of dopant in the samples prepared by combustion method is more significant than that of sol-gel.

Hwang et al. [12] have reported the presence of the second phases in the same compositions prepared at the same calcining temperatures.

The shift of the XRD peaks to lower angles shown in Figs. 2 and 3 are due to increasing of lattice constants. These changes in the lattice constants due to dopant agent originates in the substitutions of Mn^{2+} in Zn^{2+} sites which is accordance with reports given by Chattopadhyay et al. [13].

3.2 Microstructural properties

Typical TEM images of the undoped ZnO powders are shown in Fig. 4a and b. These figures show that there are

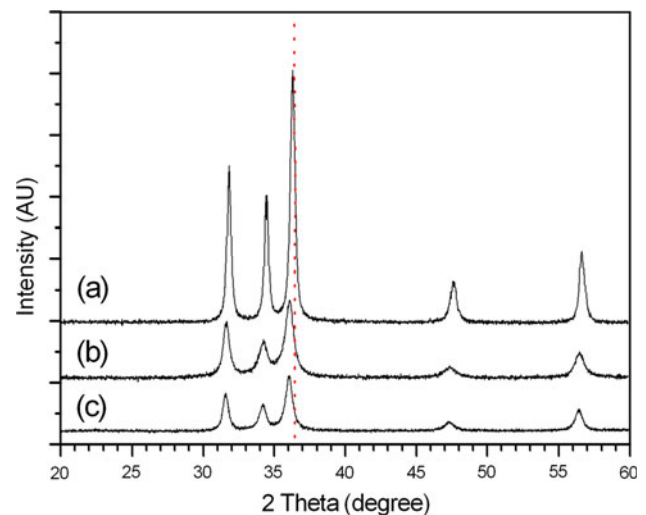


Fig. 3 XRD patterns of the $Zn_{1-x}Mn_xO$ nanopowders prepared by gel-combustion method: (a) $x = 0.00$, (b) $x = 0.06$ and (c) $x = 0.10$, calcined at $500\text{ }^\circ\text{C}$

two distinct differences in the microstructure of particles obtained by two methods. Firstly, the shape of the particles synthesized by the sol-gel method is spherical, while the shape of the particles prepared by the gel-combustion is rather hexagonal. Secondly, the average particle size of the nanopowders prepared by the gel-combustion method is smaller than that of the particles obtained by the other technique. The histograms of the particle size distribution are presented in the insets of Fig. 4a and b. As shown in these insets, the average particle size is estimated to be about 40 nm in diameters for particles prepared by the sol-gel technique, while the size of nanoparticles synthesized by gel-combustion is 25 nm . This reduction in the particle size might be due to the shorter time of gel drying process in gel-combustion method comparing to the time duration in the first method which takes several hours.

3.3 FTIR and UV analysis

The effect of doping level on the stretching, bending and vibrational modes of Zn-O and Mn-O bonds has been investigated.

The FTIR transmission spectra in terms of wavenumber for $Zn_{0.94}Mn_{0.06}O$ nanopowders prepared by sol-gel route reveal that the crystal structure has formed at $300\text{ }^\circ\text{C}$ calcining temperature. By increasing the calcining temperature, the organic decomposition occurs completely. Also, Zn-O and Mn-O stretching modes are clearly observed in Fig. 5. Two guidelines in Fig. 5a and b indicate a small shift to lower wavenumbers in the Mn-O mode of 0.06 doped nanopowder calcined at $400\text{ }^\circ\text{C}$ comparing to the similar doping level sample calcined $300\text{ }^\circ\text{C}$. This shift can be due to the elimination of tetragonal phase because of

Fig. 4 TEM images of the ZnO nanopowders prepared by **a** sol-gel and **b** gel-combustion techniques. The calcining temperature was 400 °C. The insets present the particle size distribution

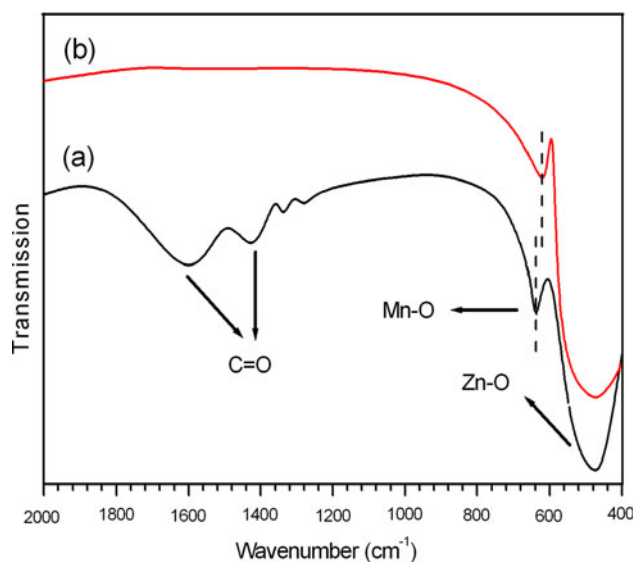
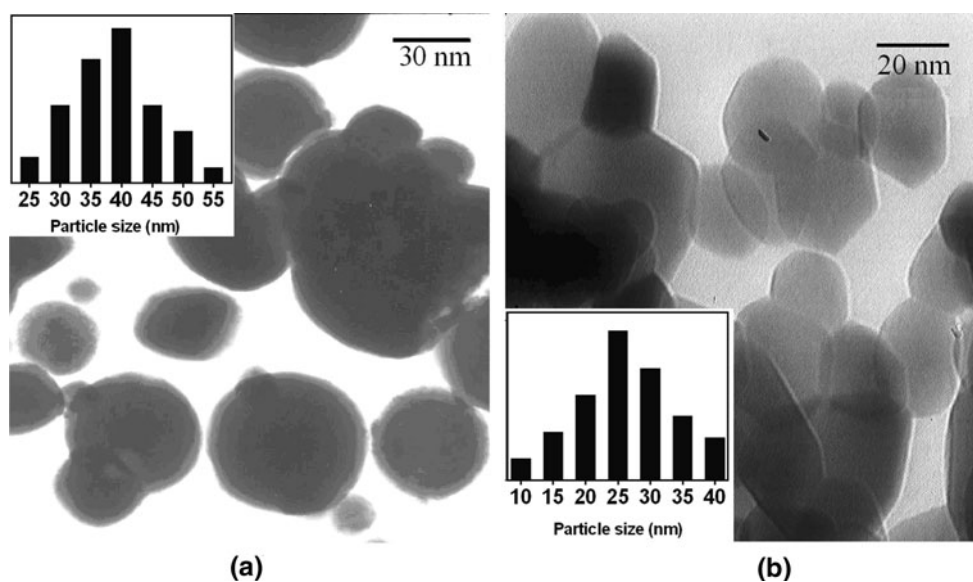


Fig. 5 FTIR transmission spectra of $\text{Zn}_{0.94}\text{Mn}_{0.06}\text{O}$ nanopowders prepared by sol-gel technique at calcining temperatures: (a) 300 °C and (b) 400 °C

increasing the calcining temperature [14]. The FTIR spectra of the samples prepared by the sol-gel and gel-combustion methods, in the region 400–1,000 cm^{-1} , are shown in Fig. 6a and b, respectively. As shown in Fig. 6a, Zn–O stretching mode is centered at about 440 cm^{-1} and also there is a shoulder at 510 cm^{-1} which are in good agreement with results reported for the sample synthesized by polymerized complex method [15] and also ZnO colloidal nanoparticles in ethanol [16]. But, there is no shoulder in the FTIR spectrum of the undoped ZnO nanopowder prepared by gel-combustion technique (Fig. 6b). In addition, Fig. 6 indicates that the absorbance band of the stretching mode corresponding to Mn–O bonds in doped

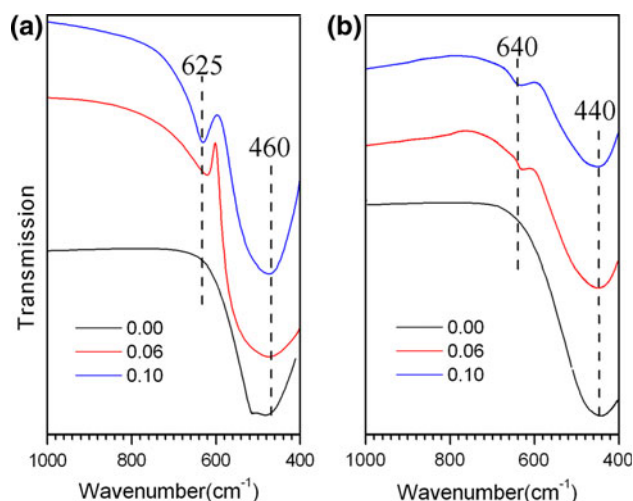


Fig. 6 FTIR transmission spectra of undoped and doped ZnO nanopowders prepared by **a** sol-gel and **b** gel-combustion techniques. The guidelines are used to clarify the absorption bands shifts

samples, obtained from sol-gel, are sharper than that of prepared by gel combustion. For a molecule to absorb IR radiation, the vibrations or rotations within a molecule cause a net change in the dipole moment of molecule. The larger this change in dipole moment, the more strongly the substance absorbs the incident radiation. Our FTIR studies show that the change in the dipole moments of Mn–O bonds in the ZnO:Mn nanopowders prepared by the gel-combustion method is small leading to the weak absorption band (around 640 cm^{-1}).

In this study, the reflectance spectra were calculated by using FTIR transmission spectra and applied to calculate the mid-IR optical properties of undoped and Mn doped specimens. The obtained values of the high frequency dielectric constant, $\epsilon(\infty)$, related to the valence electrons

Table 2 The variations in lattice constants, absorption bands centers of metal–oxygen bonds in mid-IR region and absorption edges in the UV region obtained for ZnO:Mn nanopowders due to doping and the synthesis method

Mn content	Sol–gel			Gel combustion		
	0.00	0.06	0.10	0.00	0.06	0.10
<i>XRD analysis</i>						
Lattice Const. a (Å)	3.246	3.248	3.249	3.244	3.246	3.250
Lattice Const. c (Å)	5.198	5.201	5.202	5.196	5.199	5.203
<i>FTIR analysis</i>						
Zn–O mode (cm^{-1})	456	468	468	440	446	448
Mn–O mode (cm^{-1})	–	620	626	–	630	638
$\epsilon(\infty)$	3.70	3.79	3.82	3.78	3.86	3.92
<i>UV analysis</i>						
Absorption band edge (nm)	379	385	392	375	392	406
Band gap energy (eV)	3.22	3.14	3.12	3.27	3.12	3.02

contributions are summarized in Table 2. As noted in this table, because of Mn^{2+} substitutions instead of Zn^{2+} in hexagonal structure, no striking variations in $\epsilon(\infty)$ observed with the changes in Mn doping level.

The UV absorbance spectra of undoped and Mn-doped ZnO nanopowders prepared by both methods are shown in Fig. 7. A characteristic absorption peak is distinct in all UV absorbance spectra. The absorption edge clearly shifts to longer wavelengths with the increase in Mn doping level as also reported by Shinde et al. [17].

Since the particles are nanosized and have much lower size than incident light wavelength, the absorbance spectrum is approvable to estimate the optical band gap energy, E_g . As shown in Fig. 8, a reliable method for investigating the band gap energy E_g is finding the maxima in the first derivative of absorbance spectrum with respected to the photon energy [18]. Guidelines in this figure clarify the slight reduction in the optical band gap energy values from 3.22 to 3.12 eV with the increase in Mn presence in ZnO nanopowders prepared by sol–gel technique, while the E_g values of the specimens synthesized by gel-combustion method show a vigorous decrease. Similar red-shift in band gap energy has been reported for Mn doped ZnO samples

[19]. A theoretical tight binding investigation by Olguin et al. [20] on II–VI semiconductors, suggests that the red shift is due to the increase of lattice parameters. Also, an experimental study on Mn-doped ZnO relates the band gap red shift to the band bending [13]. But, the lattice parameters of undoped and doped samples in our work are close to each other (Table 2) and it seems that the observed decreasing of the band gap energy does not originate in lattice parameters changing. On the other hand, band bending causes a slight shift in band gap energy. So in our case, it can not play a significant role on the band gap red shift. The work of Kim et al. [21] on $\text{Zn}_{1-x}\text{Co}_x\text{O}$ films shows that the decrease of the band gap energy is due to sp – d exchange interactions and dd transitions which cause the extension in ferromagnetic ordering of the samples. The decrease of the band gap energy in our samples can be due to the sp – d exchange interactions, as we have already observed the ferromagnetic state in $\text{Zn}_{0.94}\text{Mn}_{0.06}\text{O}$ [22] in agreement with Ref. [21]. The existence of the strong sp – d interactions was checked by measuring the magnetic permeability and the Curie point. In order to plot magnetic permeability versus temperature, an apparatus suggested by Cedillo et al. [23] for ferromagnetic oxides was used.

Fig. 7 Absorbance spectra in terms of wavelength for undoped and Mn-doped samples synthesized by both methods: **a** sol–gel and **b** gel-combustion. The guidelines points out the shift of absorption edge

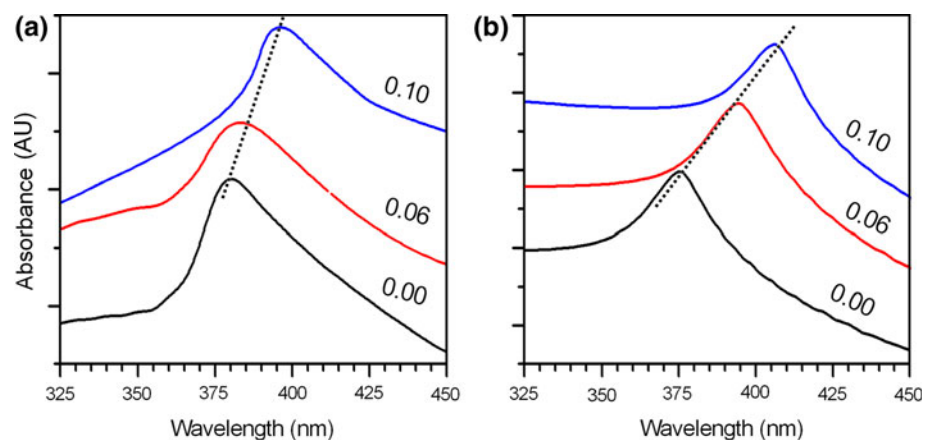


Fig. 8 First derivative of absorbance spectra in terms of photon energy calculated for undoped and Mn-doped nanopowders prepared by **a** sol-gel and **b** gel-combustion methods. The optical band gap energies are distinguished by plotting the guidelines

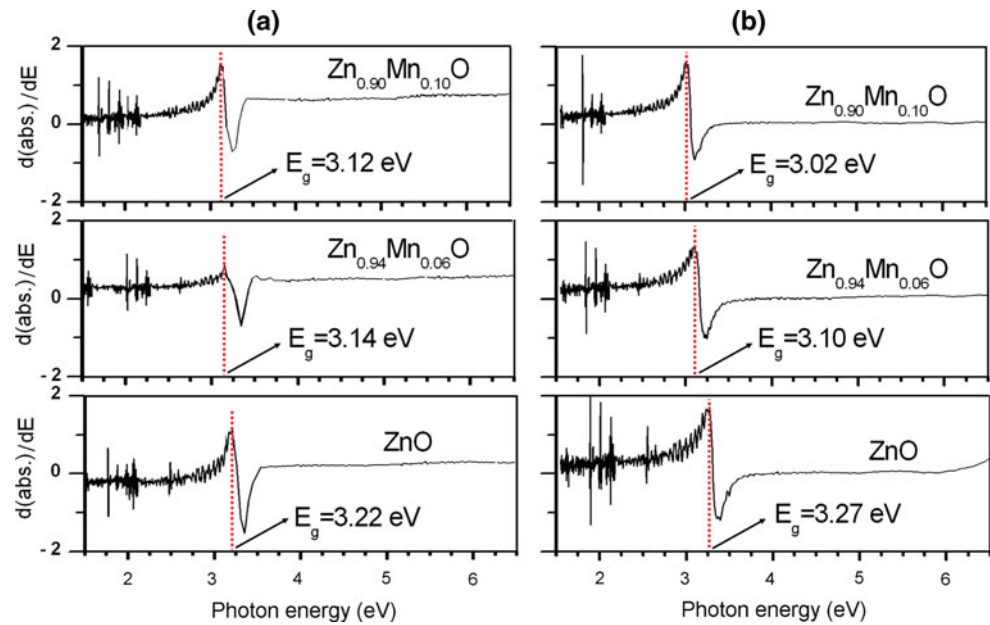


Figure 9 shows the magnetic permeability of the doped samples versus temperature. Sudden falling down the permeability in the plot presents the Curie point. As shown in this figure, the Curie temperature of the doped samples synthesized with both methods increases with the increase in Mn content. However, this figure shows the larger increase in Curie temperature of the doped samples prepared with gel-combustion method which have greater decrease in the band gap energy, comparing to the samples synthesized with the sol-gel method. So, it can be a reasonable conclusion that *sp-d* exchange interactions has

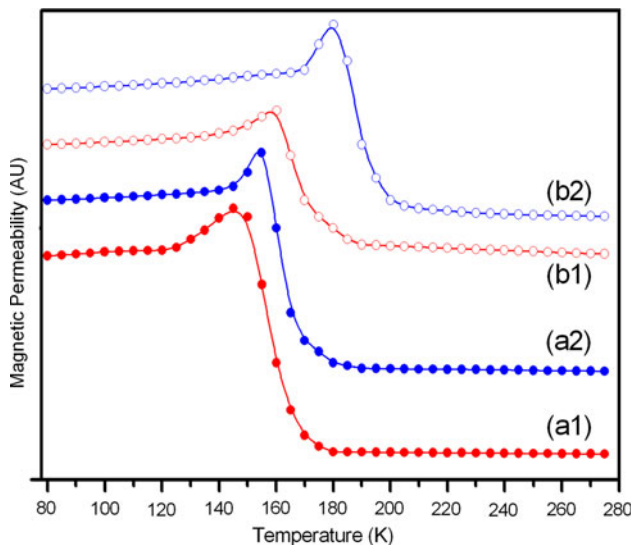


Fig. 9 Magnetic permeability versus temperature measured for $Zn_{1-x}Mn_xO$ samples prepared with both methods: (a1) $x = 0.06$ and (a2) $x = 0.10$ synthesized by sol-gel and (b1) $x = 0.06$ and (b2) $x = 0.10$ synthesized by gel-combustion method

more significant role on the band gap decreasing due to the negative and positive corrections to the conduction and valance band edges, respectively [21]. Unlike, several reports have denoted the increasing band gap energy in Mn doped ZnO comparing to undoped samples [24, 25]. Table 2 shows the comparative studies on structural and optical properties of undoped and doped ZnO nanoparticles prepared by both methods.

4 Conclusion

In this paper, undoped and Mn doped nanocrystalline ZnO have been successfully prepared by two simple methods: sol-gel and gel-combustion. The effects of doping level and synthesis process on the structural, microstructural and optical properties are discussed and from the investigations, the following conclusions can be drawn.

The XRD patterns and FTIR spectra of the doped samples imply the formation of mono-phase wurtzite type structure in the synthesized nanopowders calcining at 400 °C in sol-gel method and 500 °C in gel-combustion. TEM observations show that the morphology of nanopowders is drastically affected by synthesis route, causing the formation of either hexagonal or spherical shape particles. FTIR analysis presents that vibrational properties such as deformation of Mn–O bonds are severely affected by the preparation technique. Although, neither doping level nor changes in synthesis methods lead to observe a striking variation in amount of valance electron contribution. The UV measurements point out that the reduction in band gap energy with the increase in Mn doping level is observed in the samples prepared by both methods. But, the

decreasing rate of band gap energy due to dopant agent seems to be affected by the synthesis method.

References

1. Brus L (1990) *J Phys Chem* 90:2555–2560
2. Nepijko SA, Pippel E, Woltersdorf J (2006) *Phys Stat Sol A* 61:469–475
3. Dinesha ML, Jayanna HS, Mohanty S, Ravi S (2010) *J Alloy Compd* 490:618–623
4. Bhargava R, Sharma PK, Dutta RK, Kumar S, Panday AC, Kumar N (2010) *Mat Chem Phys* 120:393–398
5. Jung D (2010) *Solid State Sci* 12:466–470
6. Fang Y, Wen X, Yang S, Pang Q, Ding L, Wang J, Ge W (2005) *J Sol-Gel Sci Techn* 36:227–234
7. Wang J, Shi N, Qi Y, Liu M (2010) *J Sol-Gel Sci Techn* 53:101–106
8. Yang Z, Ye Z, Zhao B, Zong X, Wang P (2010) *J Sol-Gel Sci Techn* 54:282–285
9. Selim MM, Deraz NM, El-Asmi AA, Elshfay O (2010) *J Alloy Compd* 506:541–547
10. Jayakumar OD, Salunke HG, Kadam RM, Mohapatra M, Yaswant G, Kulshreshtha SK (2006) *Nanotechnology* 17:1278–1285
11. Lojkowski W, Gedanken A, Grzanka E, Opalinska A, Strachowski T, Pielaszek R, Tomaszewska-Grzeda A, Yatsunencko S, Godlewski M, Matysiak H, Kurzydowski KJ (2009) *J Nanopart Res* 11:1991–2002
12. Hwang CC, Wu TY (2004) *J Mater Sci* 39:6111–6115
13. Chattopadhyay S, Dutta S, Banerjee A, Jana D, Bandyopadhyay S, Chattopadhyay S, Sarkar A (2009) *Phys B* 404:1509–1510
14. Ebrahimizadeh Abrishami M, Hosseini SM, Kompany A (2011) *J Appl Sci* 11:1411–1415
15. Kwon YJ, Kim KH, Lim CS, Shim KB (2002) *J Ceram Process Res* 3:146–149
16. Wang H, Xie C (2008) *J Phys Chem Solids* 69:2440–2444
17. Shinde VR, Gujar TP, Lokhande CD, Mane RS, Han S-W (2006) *Mat Chem Phys* 96:326–330
18. Morales AE, Mora ES, Pal U (2007) *Rev Mex Fis* 53:18–22
19. Senthilkumaar S, Rajendran K, Banerjee S, Chini TK, Sengodan V (2008) *Mat Sci Semicon Proc* 11:6–12
20. Olguin D, Baquero R, de Coss R (2001) *Rev Mex Fis* 47:43–49
21. Kim KJ, Park YR (2002) *Appl Phys Lett* 81:1420–1422
22. Ebrahimizadeh Abrishami M, Attaran Kakhki E, Hosseini SM, Kompany A (2010) *Mod Phys Lett B* 24:749–760
23. Cedillo E, Ocampo J, Rivera V, Valenzuela R (1980) *J Phys E Sci Instrum* 13:383–386
24. Rekha K, Nirmala M, Nair MG, Anukaliani A (2010) *Phys B* 405:3180–3185
25. Deepa M, Bahadur N, Srivastava AK, Chaganti P, Sood KN (2009) *J Phys Chem Solids* 70:291–297